Aerosol and Air Quality Research, 10: 323–330, 2010

ISSN: 1680-8584 print / 2071-1409 online
doi: 10.4209/aaqr.2009.11.0074

Using Sharpness Image with Haar Function for Urban Atmospheric Visibility Measurement

Jiun-Jian Liaw[1*], Ssu-Bin Lian[1], Yung-Fa Huang[1], Rung-Ching Chen[2]

[1] *Department of Information and Communication Engineering, Chaoyang University of Technology, 168 Jifong E. Rd., Wufong Township, Taichung County, 41349, Taiwan*
[2] *Department of Information Management, Chaoyang University of Technology, 168 Jifong E. Rd., Wufong Township, Taichung County, 41349, Taiwan*

ABSTRACT

Air quality affects human health, traffic safety and human life quality. The status of air quality can be indicated by the urban atmospheric visibility. The atmospheric visibility is traditionally the human-eye observed maximum distance at which outline of the selected target can be recognized. To replace the traditional measurement for the atmospheric visibility, digital image analysis techniques provide good visibility data which is established by the numerical index. These techniques provide good performance which is defined by the correlation between the observed visual range and the obtained index. In this paper, two high pass filters for atmospheric visibility monitoring are reviewed. Since the performance is affected by non-uniform illumination, such as shadow, a scheme which is called the sharpness image with Haar function is also introduced. Synthetic images, real images and actual atmospheric images are used to show the comparison of the performances. According to the results, the introduced method obtains higher relationship with human observed visibility than the other methods. We also show that obtaining the visibility indices with the proposed procedure can increase the similarity when the observed visibilities are the same.

Keywords: Atmospheric visibility; digital image processing; Haar function; filtering.

INTRODUCTION

The influence of air quality not only affects human health, but also traffic safety and human life quality. Urban air quality is usually evaluated by the indicators such as atmospheric visibility. Low visibility strongly implies air pollution by ambient pollutants (Bishoi *et al.*, 2009), particulate matter (Lin *et al.*, 2008; Xu *et al.*, 2008), or gaseous species (Sequeira and Lai, 1998).

The visibility is the traditional measurement which is defined as the maximum distance at which the selected target can be recognized (Horvath, 1981). In other words, the atmospheric visibility is a standard of human visual perception of the environment. Many researchers have applied some photograph processing methods for measuring visibility (Malm and Molenar, 1984; Larson *et al.*, 1988) because the variation in human-eye observation could be high due to different personal characteristics (Malm, 1999). Moreover, several meters, such as the telephotometer (Agarwala *et al.*, 2004), the nephelometer and the athelometer (Jayaraman *et al.*, 2006), have also been developed to monitor visibility.

In recent years, the digital technologies are rapidly developing and applied to many applications. Digital image processing schemes have been widely used in industry, biology, pattern recognition, geographic information systems, environmental monitoring, machine vision and artificial intelligence (Luo *et al.*, 2005; Chiu and Liaw, 2006; Gonzalez and Woods, 2008), etc. Digital camera can be used to measure the predetermined distance of a target for computation of visibility (Caimi *et al.*, 2004). Expensive digital panorama camera is also used to determinate the visibility with Sobel operator (Baumer *et al.*, 2008). Digital image data can be translated to specific brightness value, the difference between the building and its background (Luo *et al.*, 2002). However, atmospheric visibility can be estimated by the digital image analysis techniques both in spatial domain and frequency domain. (Kim and Kim, 2005; Xie *et al.*, 2008).

The concept of ideal high pass filter is proposed to measure urban atmospheric visibility (Luo *et al*., 2005). The Fourier transform and the Sobel operation are used to extract high frequency data in frequency domain and spatial domain, respectively. The ideal high pass filtered

* Corresponding author. Tel.: 886-4-23323000 ext. 4755; Fax: 886-4-23305539
E-mail address: jjliaw@cyut.edu.tw

data is used to establish the visibility index. They also defined the performance by the correlation between the observed visual range and the obtained index. The correlation is the coefficient of determination, R^2, which includes linear regression. If R^2 is close to 1, it means that the correlation is high. With the ideal filter, the R^2 result is less than 0.8. However, ideal high pass filters do not easily reveal the fine structures of a non-uniform illumination area, such as the shadow, of the urban image.

Illumination and reflectance components are characteristics of the digital image. The illumination is the amount of viewed source illumination incident on the scene. The reflectance is the amount of illumination reflected by objects in the scene. Slow and fast spatial variations characterize illumination and reflectance, respectively. The homomorphic filter operates these components separately with two or more parameters. The homomorphic filter can be used to improve the ideal filter (Pratt, 2007; Gonzalez and Woods, 2008). The homomorphic filter is also used to measure the visibility. The value of R^2 of measuring the visibility index via the homomorphic filter technology is close to 0.9 (Kutner *et al.*, 2004; Sun *et al.*, 2007). According to the correlation with the observed visual range, we can see that the homomorphic filter is better than the ideal high pass filter. However, using the homomorphic filter is complex because it is necessary to decide the parameters.

To improve non-uniform illumination sharpness, an algorithm with the Haar function is proposed (Yang, 2005). Compared to the homomorphic filtering technology, this method reveals the fine structures of the non-uniform image. Since objects in the urban atmospheric image may be shaded and outlines in the dim area are not illuminated enough to be recognized, the sharpness with Haar function is suitable for measuring urban atmospheric visibility.

This paper reviews a series of digital image analysis techniques with the ideal high pass filter (Luo *et al.*, 2005) and homomorphic filter (Sun *et al.*, 2008). The current work applies the sharpness with Haar function (Yang, 2005) to estimate the visibility index. The similarity is also used to compare the performance when the observed visibilities are the same. The experiments with synthetic and real images are used to compare the proposed procedure with previous schemes.

FOURIER TRANSFORM AND IDEAL HIGH-PASS FILTER

Since impaired visibility can not be detailed, the high-frequency components in the scene decrease. The high-frequency information can be used to estimate the visibility. We can use the Fourier transform and the ideal high-pass filter to separate the high frequency components (Luo *et al.*, 2005).

The digital image can be described by a function, $f(x, y)$, where the value of the function represents the brightness level at location of (x, y). The Fourier transform of the image with $M \times N$ size can be written as (Gonzalez and Woods, 2008)

$$F(u,v) = \frac{1}{MN}\sum_{x=0}^{M-1}\sum_{y=0}^{N-1} f(x,y)\exp[-j2\pi(\frac{ux}{M}+\frac{vy}{N})] \quad (1)$$

where (u, v) are the variables in the frequency domain. The ideal 2-D high-pass filter passes high frequencies and cuts off low frequencies at the cutoff distance, D_0. The ideal high-pass filter function is defined as

$$H(u,v) = \begin{cases} 0 & if \quad D(u,v) \le D_0 \\ 1 & if \quad D(u,v) > D_0 \end{cases} \quad (2)$$

where D_0 is a positive integer and $D(u, v)$ is the distance between (u, v) and the center of the frequency domain. Finally, the filtered image can be obtained by the inverse Fourier transform. The visibility index is the average gray level of the filtered image.

HOMOMORPHIC FILTER

The ideal high pass filters do not easily reveal the fine structures of a non-uniform illumination area, such as the shadow, of the image. The homomorphic filter is useful for improving the non-uniform illumination area by brightness range compression and contrast enhancement. The homomorphic filter controls the filter function that affects low frequency and high frequency in different ways by choosing the parameters L and H. A homomorphic filter function can be defined as

$$H(u,v) = (H-L)[1-\exp(-\frac{D^2(u,v)}{D_0^2})] + L \quad (3)$$

If we assume that $L < 1$ and $H > 1$, then the filter reduces the illumination (low frequencies) and increases the reflectance (high frequencies). In this paper, we set $L = 0.5$ and $H = 1.1$. After the homomorphic filter, the data is filtered again by a 2-D Gaussian high-pass filter which is defined as

$$H(u,v) = 1-\exp(-\frac{D^2(u,v)}{2D_0^2}) \quad (4)$$

Similarly, the filtered image can be obtained by the inverse Fourier transform and the visibility index is the average gray level of the filtered image.

SHARPNESS WITH HAAR FUNCTION

The Haar function is an orthogonal base of the wavelet transform. In general, the orthogonal Haar function coefficient is typically $1/\sqrt{2}$. In other words, when two data (p_1 and p_2) are inputted, they can be separated as $(p_1 - p_2)/\sqrt{2}$ and $(p_1 + p_2)/\sqrt{2}$, respectively. In this section, we introduce how to obtain the sharpness image with Haar function (Yang, 2005).

We assume that the input image is described by a function, $f(x, y)$, where the ranges of x and y are $0 \le x < M$

and $0 \le y < N$, respectively. We compute the image in x direction and y direction. In the x direction, firstly, we set

$$p_1 = f(2m, y) \text{ and} \quad (5)$$
$$p_2 = f(2m + 1, y) \quad (6)$$

to be the two input points of the Haar function (where $0 \le m \le M/2$). We also extract one pixel shifted,

$$p_1 = f(2m + 1, y) \text{ and} \quad (7)$$
$$p_2 = f(2m + 2, y), \quad (8)$$

to operate the transformation. Similarly, the y direction proceeds two times with one pixel shifted. Two input couples of the y direction are

$$p_1 = f(x, 2n), \quad (9)$$
$$p_2 = f(x, 2n + 1) \text{ and} \quad (10)$$
$$p_1 = f(x, 2n + 1), \quad (11)$$
$$p_2 = f(x, 2n + 2), \quad (12)$$

respectively (where $0 \le n \le N/2$). We can see that the original image is separated into four subsets. In the separated subset, we set the original data (p_1 and p_2) into the sharpened data (p_1' and p_2') by the sign of the value of $(p_1 - p_2)/\sqrt{2}$. If the value is positive, we set

$$p_1' = 14\log(p_1 - p_2 + 1) \text{ and} \quad (13)$$
$$p_2' = 0, \quad (14)$$

otherwise, we set

$$p_1' = 0 \text{ and} \quad (15)$$
$$p_2' = 14\log(p_2 - p_1 + 1). \quad (16)$$

Finally, the sharpened image can be obtained by the sum of the results of four sub-images.

To estimate the visibility index, we combine the sharpened image with the homomorphic filtered image (without Gaussian high-pass filter). The combination is (the sharpened image) + c × (the homomorphic filtered image), where c is a combination weight. The same image database with Luo *et al.* (2005) is used to find the optimum value of c. The actual urban images are shot from the top of the Linden Hotel (a 42-floor building in Kaohsiung, Taiwan) to the direction of Kaohsiung City Central Area (the north east direction). At the time of shooting the image, a trained investigator also recorded observed visibility. The image database took a total 172 images (database A) with observed visibility in four months. We compute indices of all 172 images with variant c. The relation between R^2 and c is shown in Fig. 1. We can see that the best value of c is 0.78 (because it makes the highest value of R^2). It is the same with Yang (2005) suggested.

EXPERIMENTS AND RESULTS

This paper compares with the performances of the Fourier transform (with the ideal high pass filter), the homomorphic filter and the sharpness with Haar function. The experiments include synthetic images and actual atmospheric images. The following describes the summaries of the experiments and results.

The first experiment uses the synthetic images. Fig. 2(a) shows an artificial building image, Fig. 2(b) shows the same artificial building with the shadow, Fig. 2(c) is a real image of a building and Fig. 2(d) is the same real building with the shadow. The real building images are taken by the same digital camera (Nikon S1) with the same setups which are 50 sensitivity (ASA scale), 1/200 seconds exposure and F 4.4 aperture. Since the shadow should not influence visibility index, with the same method, the indices of the same target should be the same. To show performance comparisons, this paper defines the similarity with two indices, v_1 and v_2,

$$similarity = \frac{2 v_1 v_2}{v_1^2 + v_2^2} \times 100\% \quad (17)$$

We compute the visibility indices by above methods and the results (includes similarities) are shown in Table 1.

Results of the above experiments show that, the scheme of sharpness with Haar function makes the highest similarity. Since the sharpness with Haar function reduces the influence of non-uniform illumination, obtaining the visibility index by the sharpness with Haar function reduces the influence of the shadow.

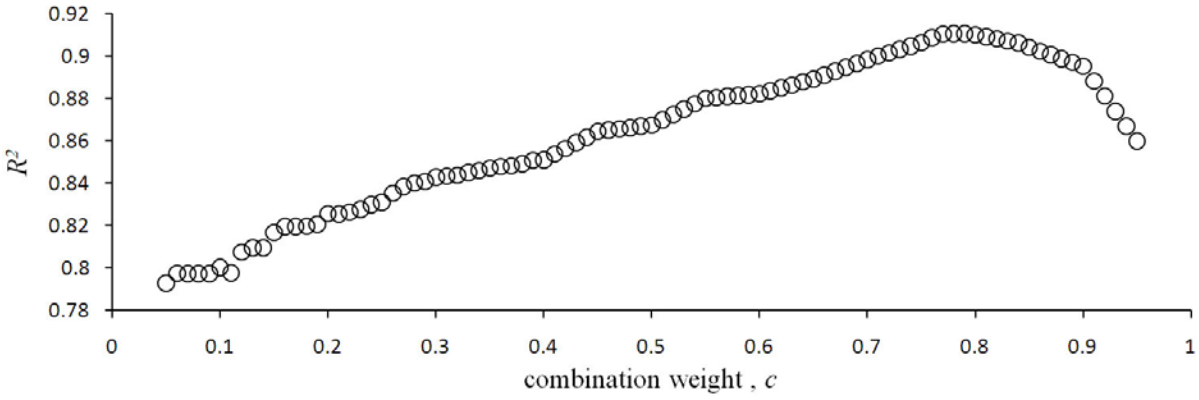

Fig. 1. The results of finding the optimum c value (the combination weight).

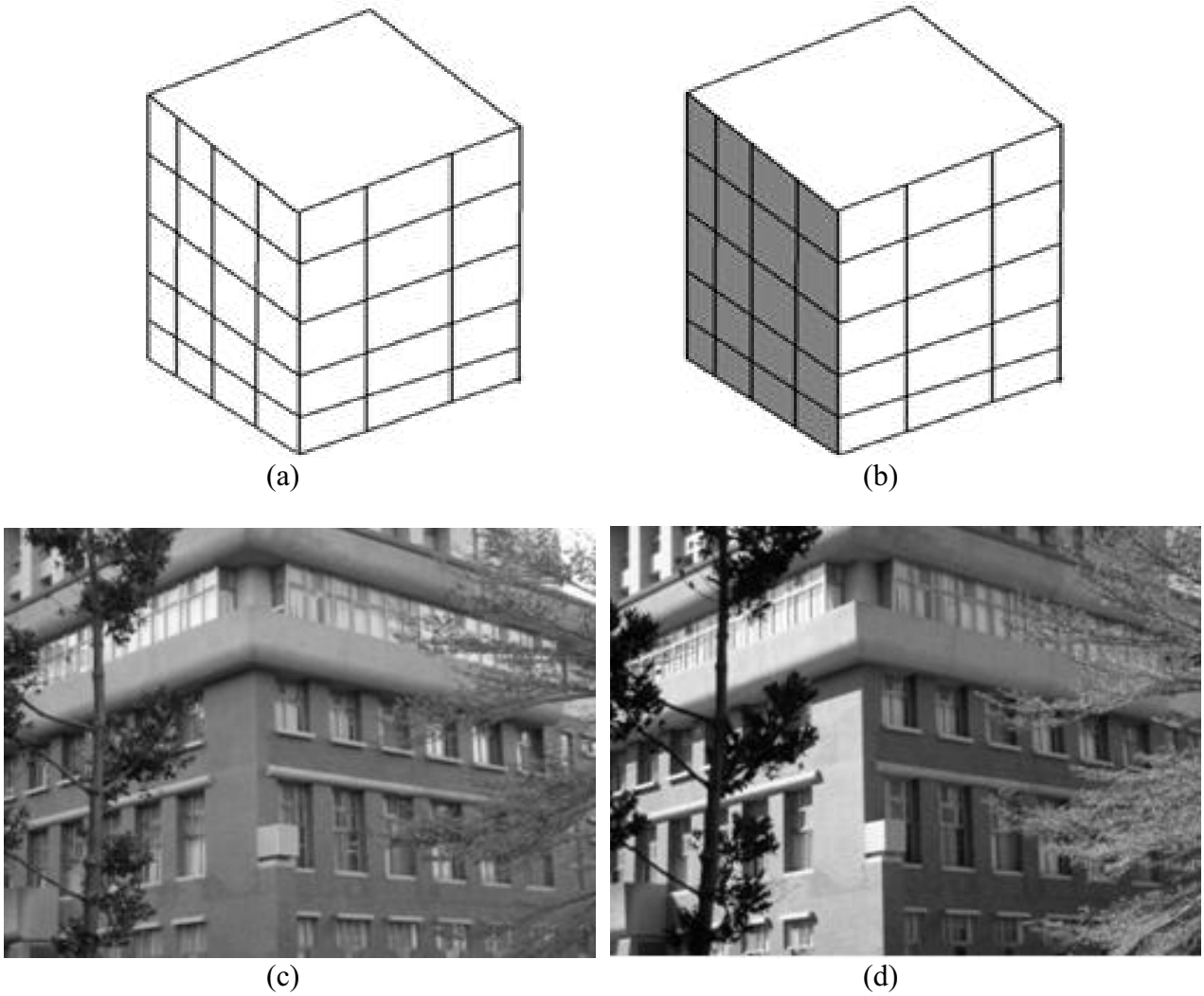

Fig. 2. The synthetic images. (a) The artificial building without shadow, (b) the artificial building with shadow, (c) the real building without shadow and (d) the real building with shadow.

Table 1. The obtained indices and similarities of the synthetic images.

Image	Fourier transform	Homomorphic filter	Sharpness with Haar function
Fig. 2(a)	26.4016	48.2157	232.8328
Fig. 2(b)	11.0367	36.4218	215.2790
similarity	71.16%	96.19%	99.70%
Fig. 2(a)	7.1020	69.7583	201.3987
Fig. 2(b)	3.9803	51.2549	183.9483
similarity	85.29%	95.43%	99.59%

This study also uses two databases of actual urban images (they are the same as in Luo *et al*. (2005)) to show the performance. The database A includes 172 images which are shot from the top of the Linden Hotel to the north east direction in Kaohsiung, Taiwan (see SHARPNESS WITH HAAR FUNCTION section). The database B includes 226 images which are shot from top of the Linden Hotel to the south direction. Two example images of the database A and B are shown in Fig. 3. The image of the database A includes many big buildings. By contrast, the buildings in the image of the database B are small and occupies less one third of the image area.

From the database A, we try to compare the similarities of the three methods with shaded buildings compared to no shaded buildings in the same observed visibility. Fig. 4(a) shows an urban image obtained with less shadow. Fig. 4(b) shows another image and we can see that Fig. 4(b) shows more shaded buildings than Fig. 4(a). The observed visibilities of Fig. 4(a) and Fig.4 (b) are the same (3 km). Fig. 4(c) and Fig. 4(d) show the images with 5 km observed visibility. Fig. 4(e) and Fig. 4(f) show the images with 12 km observed visibility. Similar to above, Fig. 4(c) and Fig.4 (e) are images of the less shadowed buildings and Fig. 4(d) and Fig. 4(f) are images of the more shadowed buildings. Since human observed visibilities are the same, indices similarity with the same method should be closed to 100%. Table 2 shows the results of computing visibility indices by the three methods. Similar to the above results, the similarity of the sharpness with Haar function is the best.

The results of the above comparisons show that the proposed scheme reduces the influence of non-uniform illumination (shadow). Obtaining the visibility indices with the sharpness with Haar function can increase the similarity when the observed visibilities are the same.

Finally, this study computes the indices of database A and B. Relationships between observed visibility values and the computed indices show the performance. The correlation, which is the coefficient of determination, R^2, defines the relationship. If R^2 is close to 1, it means that

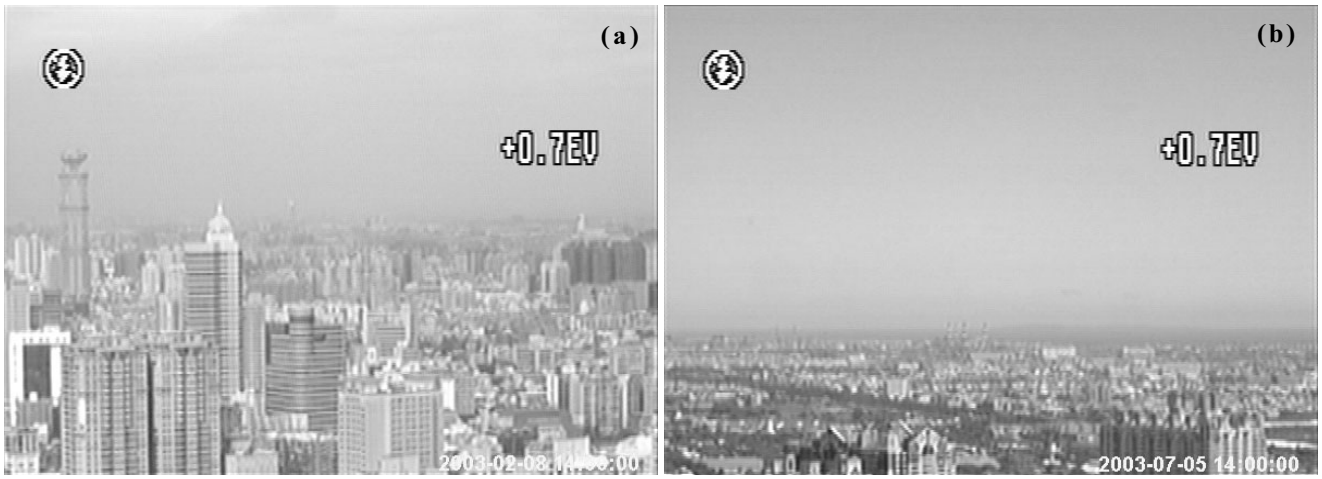

Fig. 3. The example images. (a) an image of database A and (b) an image of database B.

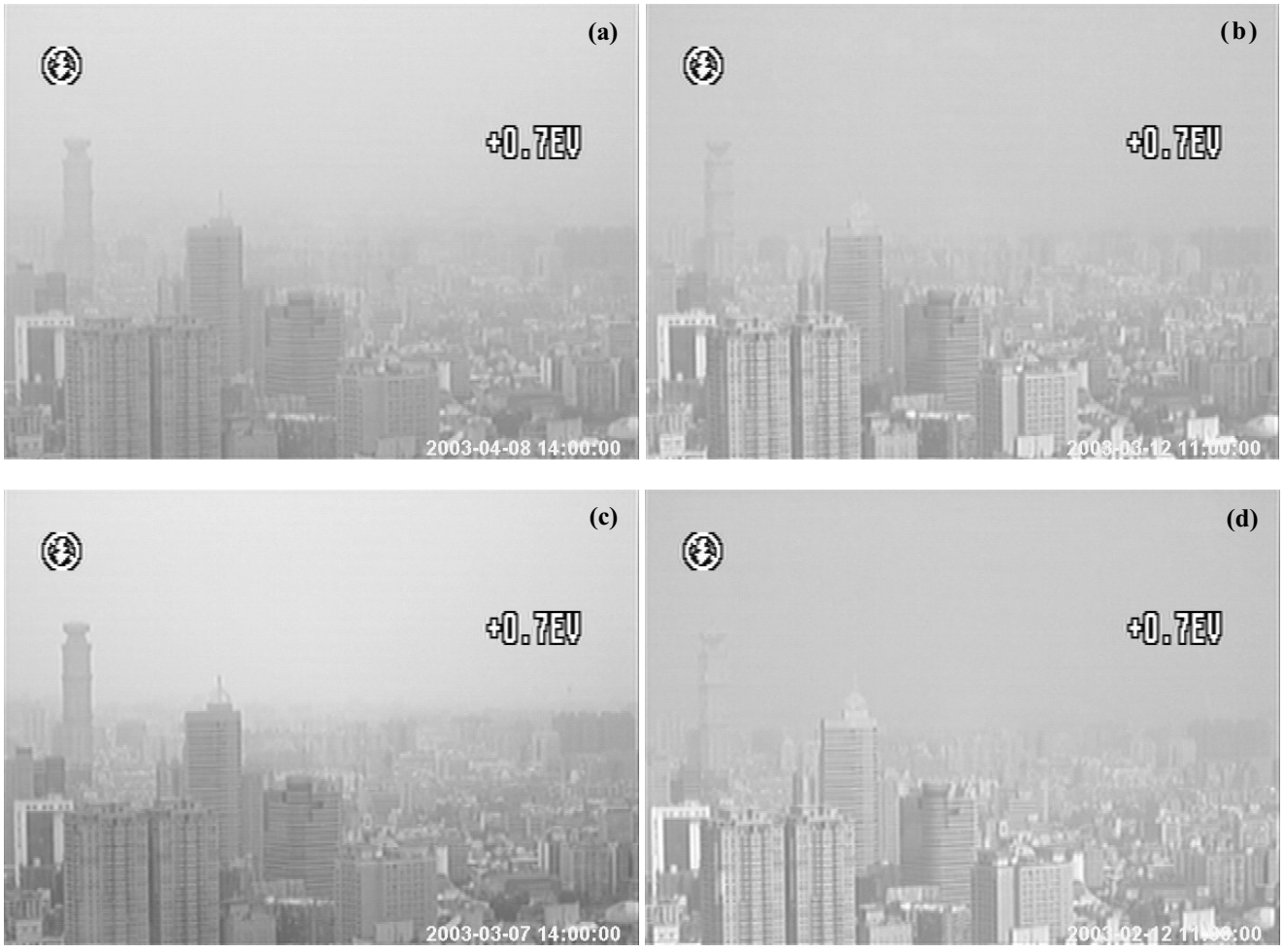

Fig. 4. The actual urban images (with different observed visibilities) which are shot on cloudy day and sunny day. (a) 3 km without shadow, (b) 3 km with shadow, (c) 5 km without shadow, (d) 5 km with shadow, (e) 12 km without shadow, and (f) 12 km with shadow.

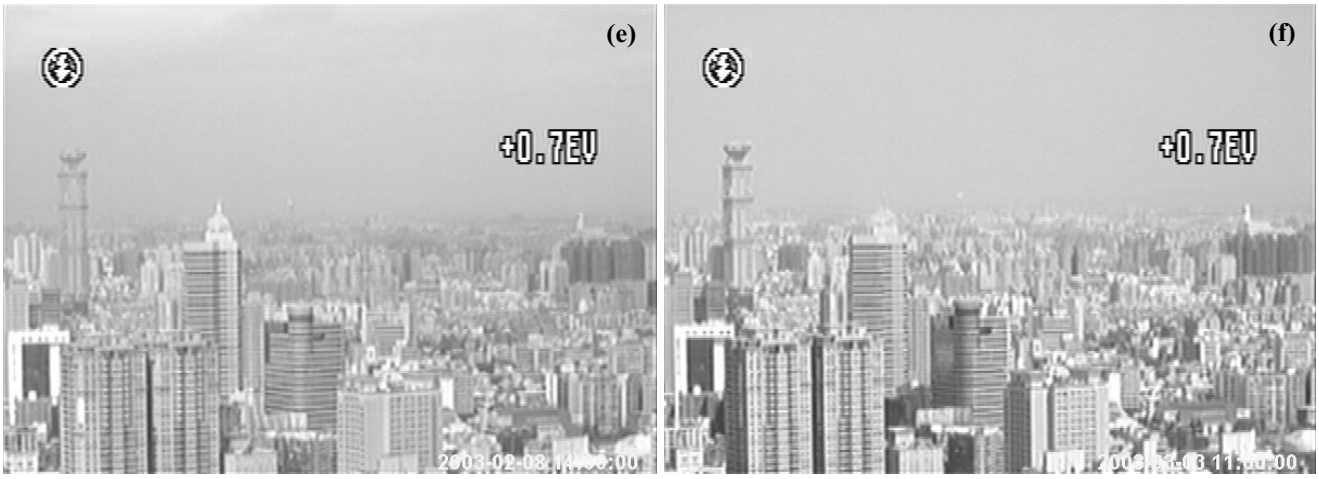

Fig. 4. *(continue)*.

Table 2. The obtained indices and similarities of the actual urban images.

Image	Fourier transform	Homomorphic filter	Sharpness with Haar function
Fig. 4(a)	13.3632	18.9564	128.5871
Fig. 4(b)	9.8486	22.4225	135.5449
similarity	95.51%	98.60%	99.86%
Fig. 4(c)	19.7562	29.3877	146.2156
Fig. 4(d)	10.6521	24.2651	143.3134
similarity	83.54%	98.19%	99.97%
Fig. 4(e)	21.1721	37.8422	165.3027
Fig. 4(f)	32.8473	49.6731	179.5326
similarity	91.07%	96.41%	99.93%

the relationship is high. Fig. 5 and Fig. 6 show the relationships (by three methods) with database A and B, respectively. The line equations of the linear regression and R^2 are also shown on the figure. In the results of database A, we can find that the performances of the Fourier transform (with ideal high pass filter), the homomorphic filter and the sharpness with Haar function are R^2 = 0.77, R^2 = 0.86, and R^2 = 0.91, respectively. Similarly, in the results of database B, we can find that the performances of the Fourier transform (with ideal high pass filter), the homomorphic filter and the sharpness with Haar function are R^2 = 0.70, R^2 = 0.81, and R^2 = 0.87, respectively. According to the experiment results, the proposed procedure, the sharpness with Haar function, obtains the higher relationship with human observed visibility than the other methods. Moreover, since the performance of the database A (the images with many big buildings) is higher than the database B, the sharpness with Haar function is more suitable for the case of the urban atmospheric visibility measurement which the image includes many big buildings.

CONCLUSIONS

This paper introduces a series of digital image analysis schemes, based on high pass filters, for urban atmospheric visibility monitoring. Since the urban atmospheric images may be shaded and outlines in the dim area are not illuminated enough to be recognized, this paper introduces a procedure which is based on a sharpness of the non-illumination image. The experiments in this study use synthetic images, real images and actual atmospheric images to show the comparison of the performances between the Fourier transform, the homomorphic filter and the introduced procedure, the sharpness with Haar function. The performance is defined by the correlation, R^2, between the observed visual range and the obtained index. Results show that the sharpness with Haar function obtains higher relationship with human observed visibility than the other methods. We also show that obtaining the visibility indices with the proposed procedure can increase the similarity when the observed visibilities are the same. The sharpness with Haar function is more suitable for the case of the urban atmospheric visibility measurement.

ACKNOWLEDGEMENT

The authors would like to thank Dr. Chung-Shin Yuan and Dr. Chin-Hsiang Luo for providing the experiment samples (database A and B). This study is supported partially by the National Science Council of Republic of China, Taiwan, NSC 97-2221-E-324-041.

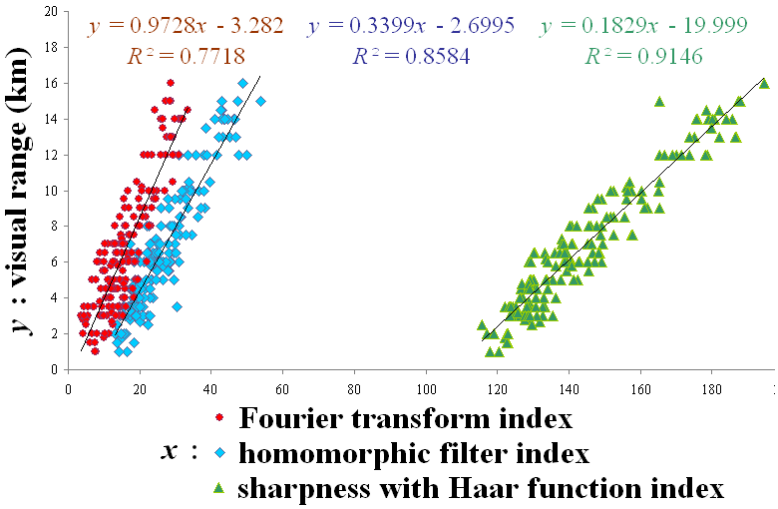

Fig. 5. The result of actual urban images with database A.

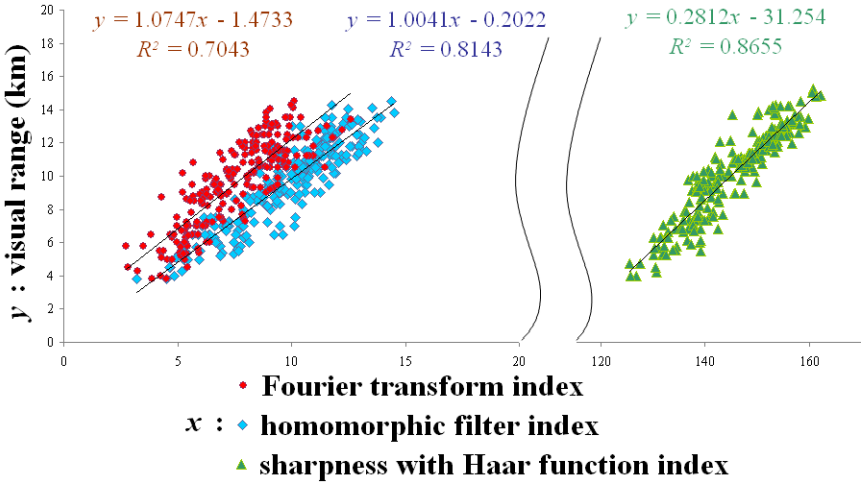

Fig. 6. The result of actual urban images with database B.

REFERENCES

Agarwala, A., Dontcheva, M., Agrawala, M., Drucker, S., Colburn, A., Curless, B., Salesin, D. and Cohen, M. (2004). Interactive Digital Photomontage. *ACM Trans. Graphics.* 23: 294–302.

Baumer, D., Versick, S. and Vogel, B. (2008). Determination of the Visibility Using a Digital Panorama Camera. *Atmos. Environ.* 42: 2593–2602.

Bishoi, B., Prakash, A. and Jain, V.K. (2009). A Comparative Study of Air Quality Index Based on Factor Analysis and US-EPA Methods for an Urban Environment. *Aerosol Air Qual. Res.* 9: 1–17.

Caimi, F., Kocak, D. and Justak, J. (2004). Remote Visibility Measurement Technique Using Object Plane Data from Digital Image Sensors, Proc. IEEE Int. Geosci. Remote. Sens., Alaska, U.S.A., 2004, p. 3288–3291.

Chiu, S.H. and Liaw, J.J. (2006). A Proposed Circle/Circular Arc Detection Method Using the Modified Randomized Hough Transform. *J. Chin. Inst. Eng.* 15: 533–538.

Gonzalez, R.C. and Woods, R.E. (2008). *Digital Image Processing*, Pearson Prentice Hall, U.S.A.

Horvath, H. (1981). Atmospheric Visibility. *Atmos. Environ.* 15: 1785–1796.

Jayaraman, A., Gadhavi, H., Ganguly, D., Misra, A., Ramachandran, S. and Rajesh, R.A. (2006) Spatial Variations in Aerosol Characteristics and Regional Radiative Forcing over India: Measurements and Modeling of 2004 Road Campaign Experiment. *Atmos. Environ.* 40: 6504–6515.

Kim, K. and Kim, Y. (2005). Perceived Visibility Measurement Using the HSI Color Different Method. *J. Korean Phys. Soc.* 46: 1243–1250.

Kutner, M., Nachtsheim, C. and Neter J. (2004). *Applied Linear Regression Models*, McGraw-Hill, U.S.A.

Larson, S.M., Cass, G.R., Hussey, K.J. and Luce, F. (1988). Verification of Image Processing Based Visibility Models. *Environ. Sci. Technol.* 22: 629–637.

Lin, C.H., Wu, Y.L., Lai, C.H., Watson, J.G. and Chow, J.C. (2008). Air Quality Measurements from the

Southern Particulate Matter Supersite in Taiwan. *Aerosol Air Qual. Res.* 8: 233–264.

Luo, C.H., Lee, W.M.G., Lai, Y.C., Wen, C.Y. and Liaw, J.J. (2005). Measuring the Fractal Dimension of Diesel Soot Agglomerates by Factional Brownian Motion Processor. *Atmos. Environ.* 39: 3565–3572.

Luo, C.H., Liu, S.H. and Yuan, C.S. (2002). Investigate Atmospheric Visibility by the Digital Telephotography. *Aerosol Air Qual. Res.* 2: 23–29.

Luo, C.H., Wen, C.Y., Yuan, C.S., Liaw, J.J., Lo, C.C. and Chiu, S.H. (2005). Investigation of Urban Atmospheric Visibility by High-frequency Extraction: Model Development and Filed Test. *Atmos. Environ.* 39: 2545–2552.

Malm, W.C. (1999). *Introduction to Visibility*, Cooperative Institute for Research in the Atmosphere, Colorado State University.

Malm, W.C. and Molenar, J.V. (1984). Visibility Measurements in National Parks in the Western United States. *J. Air Pollut. Contr. Assoc.* 34: 899–904.

Pratt, W.K. (2007). *Digital Image Processing: PIKS Scientific Inside, 4th Edition*, Wiley-Interscience, U.S.A.

Sequeira, R. and Lai, K.H. (1998). The Effect of Meteorological Parameters and Aerosol Constituents on Visibility in Urban Hong Kong. *Atmos. Environ.* 32: 2865–2877.

Sun, Y.C., Liaw, J.J. and Luo, C.H. (2007). Measuring Atmospheric Visibility Index by Different High-pass Operations, Proc. Comput. Vis. Graph. Image Process., Miao-Li, Taiwan, 2007, p. 423–428.

Xie, L., Chiu, A. and Newsam, S. (2008). Estimating Atmospheric Visibility Using General-Purpose Cameras. *Lect. Notes Comput. Sci. (LNCS)* 5359: 356–367.

Xu, S., Barsha, N.A.F. and Li, J. (2008). Analyzing Regional Influence of Particulate Matter on the City of Beijing, China. *Aerosol Air Qual. Res.* 8: 78–93.

Yang, C.C. (2005). Improving the Sharpness of an Image with Non-uniform Illumination. *Opt. Laser Technol.* 37: 235–238.

Received for review, November 29, 2009
Accepted, March 18, 2010